AFRL-RX-WP-TP-2009-4094

APPLICATION OF A TERNARY PHASE-FIELD MODEL TO PRECIPITATION BEHAVIOR IN Ni-Al-Cr ALLOYS (PREPRINT)

J.P. Simmons, C. Woodward, and Y.H. Wen

Metals Branch
Metals, Ceramics and NDE Division

APRIL 2009

AIR FORCE RESEARCH LABORATORY
MATERIALS AND MANUFACTURING DIRECTORATE
WRIGHT-PATTERSON AIR FORCE BASE, OH 45433-7750
AIR FORCE MATERIEL COMMAND
UNITED STATES AIR FORCE

REPORT DOCUMENTATION PAGE

Form Approved
OMB No. 0704-0188

1. REPORT DATE *(DD-MM-YY)*	2. REPORT TYPE	3. DATES COVERED *(From - To)*
April 2009	Journal Article Preprint	01 April 2009- 01 April 2009

4. TITLE AND SUBTITLE
APPLICATION OF A TERNARY PHASE-FIELD MODEL TO PRECIPITATION BEHAVIOR IN Ni-Al-Cr ALLOYS (PREPRINT)

5a. CONTRACT NUMBER
In-house

5b. GRANT NUMBER

5c. PROGRAM ELEMENT NUMBER
62102F

6. AUTHOR(S)
J.P. Simmons and C. Woodward (AFRL/RXLMD)
Y.H. Wen (UES, Inc.)

5d. PROJECT NUMBER
4347

5e. TASK NUMBER
RG

5f. WORK UNIT NUMBER
M02R1000

7. PERFORMING ORGANIZATION NAME(S) AND ADDRESS(ES)

Metals Branch (RXLMP)
Metals, Ceramics and NDE Division
Materials and Manufacturing Directorate
Wright-Patterson Air Force Base, OH 45433-7750
Air Force Materiel Command, United States Air Force

UES, Inc.
4401 Dayton-Xenia Road
Dayton, OH 45432

8. PERFORMING ORGANIZATION REPORT NUMBER
AFRL-RX-WP-TP-2009-4094

9. SPONSORING/MONITORING AGENCY NAME(S) AND ADDRESS(ES)
Air Force Research Laboratory
Materials and Manufacturing Directorate
Wright-Patterson Air Force Base, OH 45433-7750
Air Force Materiel Command
United States Air Force

10. SPONSORING/MONITORING AGENCY ACRONYM(S)
AFRL/RXLMD

11. SPONSORING/MONITORING AGENCY REPORT NUMBER(S)
AFRL-RX-WP-TP-2009-4094

12. DISTRIBUTION/AVAILABILITY STATEMENT
Approved for public release; distribution unlimited.

13. SUPPLEMENTARY NOTES
To be submitted to Acta Mater (Elsevier)
PAO Case Number and clearance date: 88ABW-2009-0068, 12 January 2009.

14. ABSTRACT
A recently developed ternary phase-field model is applied to study the precipitation behavior in Ni-Al-Cr alloys. The effect of diffusivity and initial compositional/ordering profiles on the growth process of precipitates are examined. Specifically, the composition evolution with time in the precipitates is simulated and compared with experimental observations by Sudbrack et al. The simulation work reveals that the CR- trapping phenomenon can only be reproduced with no significant partitioning of Cr at the nucleation stage. By looking into the composition dependent diffusivity and thermodynamic driving force for both Al and Cr, it is found that the key difference resides in the much stronger composition dependence of the diffusivity of Al.

15. SUBJECT TERMS
ageing, Ni-Al-Cr alloys, ternary phase field models, precipitation, Cr-trapping

16. SECURITY CLASSIFICATION OF:			17. LIMITATION OF ABSTRACT:	18. NUMBER OF PAGES	19a. NAME OF RESPONSIBLE PERSON (Monitor)
a. REPORT	b. ABSTRACT	c. THIS PAGE			Christopher F. Woodward
Unclassified	Unclassified	Unclassified	SAR	26	19b. TELEPHONE NUMBER *(Include Area Code)* N/A

Standard Form 298 (Rev. 8-98)
Prescribed by ANSI Std. Z39-18

Application of a Ternary Phase-Field Model to Precipitation Behavior in Ni-Al-Cr Alloys

Y.H. Wen[a,b], J.P. Simmons[a], C. Woodward[a]

[a] *Air Force Research Laboratory, AFRL/RXLM, Wright-Patterson AFB, OH 45433, USA*

[b] *UES,Inc., 4401 Dayton-Xenia Road, Dayton, OH 45432, USA*

Abstract

A recently developed ternary phase-field model [Wen et al., Acta Mater. submitted] is applied to study the precipitation behavior in Ni-Al-Cr alloys. The effect of diffusivity and initial compositional/ordering profiles on the growth process of precipitates are examined. Specifically, the composition evolution with time in the precipitates (γ') is simulated and compared with experimental observations by Sudbrack et al. [Acta mater., **54**:3199,2006]. The simulation work reveals that the Cr-trapping phenomenon can only be reproduced with no significant partitioning of Cr at the nucleation stage. By looking into the composition dependent diffusivity and thermodynamic driving force for both Al and Cr, it is found that the key difference resides in the much stronger composition dependence of the diffusivity of Al. The diffuvisity of Al is enhanced by roughly an order of magnitude across regions near or at a γ/γ' interface region. On the contrary, the diffusivity of Cr does not show a strong composition dependence. This is believed to be the major factor that has caused Cr being left 'trapped' during the growth of the precipitate while Al approaching to the equilibrium concentration quickly to minimize the total energy.

Key words: ageing, Ni-Al-Cr alloys, ternary phase-field models, precipitation, Cr-trapping

1 Introduction

The compositional evolution inside the γ'-precipitate and γ-matrix was recently measured with atom-probe tomography for Ni-5.2 Al-14.2 Cr at.% specimens aged at 873K [1]. The results were analysed by comparing with CALPHAD assessments. The measured values were largely in line with CALPHAD predictions. For example, the experimental values for the equilibrium composition of the γ-matrix are near the CALPHAD predictions. The observed

decreasing concentration of Al in the interior of the γ'-precipitate with time followed the same trend as predicted by CALPHAD. The most striking discrepancy was, however, the evolution of Cr concentration in the γ'-precipitate. The observed concentration of Cr in the precipitate decreases monotonically with the growth of the precipitate while the CALPHAD approach predicts the opposite. This phenomenon was referred to as Cr-trapping. The objective of this work is to understand the mechanism behind the Cr-trapping phenomenon using our recently developed ternary phase-field model [2].

The observed trend in Cr concentration in the precipitate was attributed to the kinetically trapped Cr atoms [3] based on a mean field evaluation that the intrinsic diffusivity of Cr is slightly smaller than that of Al [4]. This difference in diffusivity is, however, not significant enough to be the sole factor to cause such a dramatic change in the trend of the Cr evolution in the γ'-precipitat. Sudbrack et al [3] reported the presence of Ni_3Al-type $L1_2$ short range ordering domains in the as-quenched alloy, which was most likely resulted from fast Al diffusion during the quench from the solutionizing temperature of 1123K. It is speculated that the initial inhomogeneity in structure/composition may have played an important role in the nucleation of γ'-precipitate resulting in a change in the evolution behavior of Cr with the growth of the precipitate. Another possible factor is the thermodynamic driving force considering that the diffusion is controlled by the product of the diffusion mobility and the gradient of the thermodynamic driving force. The driving force might be much smaller for Cr diffusion as compared to that for Al diffusion. As such, the Cr-trapping could be mainly a thermodynamic effect rather than a kinetic one. In summary, the Cr-trapping could at least be attributed to three factors, i.e. smaller diffusivity of Cr, some kind of favorable initial nucleus structural/compositional profiles, and smaller thermodynamic driving force for Cr diffusion. It should be pointed out that these three factors are interrelated. For example, the initial nucleus structural/compositional profiles may be largely determined by defect structure of the solute solution, which is strongly affected by the specific heat treating of the sample, e.g. the cooling rate. But it can also be controlled by the thermodynamic driving force and diffusivity of Al and Cr. The focus of this work is to identify the most dominant factor that has caused the Cr-trapping phenomenon. In what follows, the ternary phase-field model is described and some simulation results and a brief discussion are presented in Sec.3.

2 The ternary phase-field model

A more detailed description of our ternary phase-field model was given elsewhere [2]. The model linked directly to commercial CALPHAD software. A diffusion mobility database was implemented that included the contribution from the ordered state allowing us to have a better description of diffusion

behavior near the γ/γ' interfaces and inside the ordered γ' phase. The misfit effects of the partitioning of the two solute elements were also taken into account.

Six long-range order (*lro*) parameters, *i.e.* $\eta_n^k(\mathbf{r},t)$ and two concentration field variables $x_n(\mathbf{r},t)$ are used to describe the two-phase microstructure $(\gamma+\gamma')$ in the Ni-Al-Cr systems [2]. Here $k=1,2,3$ are the three components of *lro* parameters. $n=1,2$ representing Al and Cr, respectively. $\mathbf{r}$ and t are spatial coordinates and time. These eight field variables can fully describe the concentration inhomogeneity of solute Al and Cr in the two phases and their site fractions in the ordered domain structures in γ'.

The microstructural evolution can be simulated by solving the time-dependent Ginzburg-Landau equation for the six *lro* parameters and using the non-linear Cahn-Hilliard diffusion equation for the two concentration fields:

$$\frac{\partial \eta_i^p}{\partial t} = -L\frac{\delta F}{\delta \eta_i^p}; \tag{1}$$

$$\frac{\partial x_i}{\partial t} = V_m^2 \nabla\left[\sum_j M_{ij}\left(\nabla\frac{\delta F}{\delta x_j}\right)\right], \tag{2}$$

where L is the structural relaxation constant, M_{ij} are the diffusion mobilities, V_m is the molar volume, and F is the total free energy of the system.

For the coherent precipitation under consideration, the total free energy consists of the elastic strain energy (F_{el}) and the chemical free energy (F_{ch}):

$$F = F_{el} + F_{ch} \tag{3}$$

The elastic strain energy arises because of the lattice mismatch between the γ and γ' phases. The misfit strain is assumed to depend on the compositions of the two solute elements in the two phases. The elastic energy of a two-phase mixture can then be calculated as a function of the concentration profiles [2]:

$$\begin{aligned} F_{el} = {} & \frac{V}{2} C_{ijkl}\overline{\epsilon}_{ij}\overline{\epsilon}_{kl} - VC_{ijkl}\overline{\epsilon}_{ij}\sum_{p=1}^{2}\epsilon_{kl}^{\circ}(p)\,\overline{\Delta x_p} \\ & + \frac{V}{2} C_{ijkl}\sum_{p=1}^{2}\sum_{q=1}^{2}\epsilon_{ij}^{\circ}(p)\,\epsilon_{kl}^{\circ}(q)\,\overline{\Delta x_p \Delta x_q} \\ & - \frac{1}{2}\sum_{p=1}^{2}\sum_{q=1}^{2}\int'\frac{d^3\mathbf{g}}{(2\pi)^3} B_{pq}(\mathbf{n})\,\{\Delta x_p\}_{\mathbf{g}}^{*}\{\Delta x_q\}_{\mathbf{g}}, \end{aligned} \tag{4}$$

where $\left(\overline{A}\right)$ is the average volume of (A), V is the total volume of the system, C_{ijkl} is the elastic moduli tensor, $\epsilon_{ij}^{\circ}(p)$ is the stress free transformation strain tensor associated with the partitioning of solute p, Δx_p is the deviation of the

local concentration of solute p from its bulk concentration. The notation $\int'$ indicates that the point $n = 0$ is excluded from the integration, and $B_{pq}(\mathbf{n})$ is a two-body interaction potential given by:

$$B_{pq}(\mathbf{n}) = n_i \sigma^{\circ}_{ij}(p)\, \Omega_{jk}(\mathbf{n})\, \sigma_{kl}(q) n_l, \tag{5}$$

where $n = \frac{\mathbf{g}}{|\mathbf{g}|}$ is a unit vector in reciprocal space and n_i is the ith component, $\sigma^{\circ}_{ij} = C_{ijkl}\epsilon^{\circ}_{kl}(p)$ and $\Omega_{ij}(\mathbf{n})$ is a Green function tensor which is inverse to the tensor $\Omega^{-1}_{ij}(\mathbf{n}) = C_{ijkl} n_k n_l$, $\{\Delta x_p\}_g$ is the Fourier transform of Δx_p, and $\{\Delta x_p\}^*_g$ is the complex conjugate of $\{\Delta x_p\}_g$.

The chemical free energy consists of the local chemical free energy and the gradient terms arising from compositional and structural inhomogeneities [5], i.e.,

$$F_{ch} = \int_V \left[f(x_{Al}, x_{Cr}, \eta^p_{Al}, \eta^p_{Cr}, T) + \frac{1}{2} \sum_{i,j=Al,Cr} \left(\kappa_{x_{ij}} \nabla x_i \nabla x_j \right) \right. \tag{6}$$
$$\left. + \frac{1}{2} \kappa_\eta \sum_{i=Al,Cr} \sum_p (\nabla \eta^p_i)^2 \right] dV$$

where $f(x_{Al}, x_{Cr}, \eta^p_{Al}, \eta^p_{Cr}, T)$ is the local chemical free energy that defines the basic thermodynamic properties of the system, $\kappa_{x_{ij}}$ and κ_η are gradient energy coefficients, and it is understood that $p = 1, 2, 3$ for the three components of the *lro* parameters.

In the CALPHAD method, the local chemical free energy is expressed as a sum of a reference free energy, an ideal mixing free energy, and excess mixing free energy:

$$G(\mathbf{r}, T) = G^{ref}(\mathbf{r}, T) + G^{id}(\mathbf{r}, T) + G^{ex}(\mathbf{r}, T). \tag{7}$$

The three energy terms depend on the site fractions of the two solute elements as follows:

$$\begin{aligned}
G^{ref}(\mathbf{r}, T) &= \sum_{i=1}^{N} \sum_{j=1}^{N} \sum_{k=1}^{N} \sum_{l=1}^{N} y^1_i(\mathbf{r})\, y^2_j(\mathbf{r})\, y^3_k(\mathbf{r})\, y^4_l(\mathbf{r})\, G^{\circ}_{ijkl}(T); \\
G^{id}(\mathbf{r}, T) &= RT \sum_{s=1}^{4} f^s \sum_{n=1}^{N} y^s_n(\mathbf{r}) \ln\left[y^s_n(\mathbf{r})\right]; \\
G^{ex}(\mathbf{r}, T) &= \sum_{s=1}^{4} \sum_{t \neq s}^{4} \sum_{p=1}^{N} y^s_p(\mathbf{r}) \sum_{q=1}^{N} y^s_q(\mathbf{r})\, y^t_p(\mathbf{r}) \cdot \sum_{m=1}^{N_{ipq}} [y^s_p(\mathbf{r}) - y^s_q(\mathbf{r})]^m G^{st}_{pq}(m, T),
\end{aligned} \tag{8}$$

where N is the total number of elements in the alloy, and $y^s_i(\mathbf{r})$ is the site fraction of element i on sublattice s with normalizations $\sum_{p=1}^{N} y^s_p(\mathbf{r}) = 1$ and $\frac{1}{4}\sum_{s=1}^{4} y^s_p(\mathbf{r}) = x_p$; that is, summing the fractional occupancies over all the

alloying elements on each sublattice must equal one, and summing the fractional occupancies over all sublattices for each alloying element must equal the mole fraction of that element. The functions $G^{\circ}_{ijkl}(T)$ and $G^{st}_{pq}(m,T)$ are empirically fitted parameters tabulated as functions of temperature in thermodynamic databases. R is the gas constant, f^s is the site fraction of sublattice s.

The local chemical free energy in Eq. 7 is expressed as a function of the site fractions of the elements on each of the four sublattices. However, in the phase-field description the local chemical free energy is a function of local concentrations and *lro* parameters. The two set of parameters are related to each other as described below:

$$\begin{aligned}
y^1_n(\mathbf{r},t) &= x_n(\mathbf{r},t)\left[1+\eta^1_n(\mathbf{r},t)+\eta^2_n(\mathbf{r},t)+\eta^3_n(\mathbf{r},t)\right] \\
y^2_n(\mathbf{r},t) &= x_n(\mathbf{r},t)\left[1-\eta^1_n(\mathbf{r},t)-\eta^2_n(\mathbf{r},t)+\eta^3_n(\mathbf{r},t)\right] \\
y^3_n(\mathbf{r},t) &= x_n(\mathbf{r},t)\left[1-\eta^1_n(\mathbf{r},t)+\eta^2_n(\mathbf{r},t)-\eta^3_n(\mathbf{r},t)\right] \\
y^4_n(\mathbf{r},t) &= x_n(\mathbf{r},t)\left[1+\eta^1_n(\mathbf{r},t)-\eta^2_n(\mathbf{r},t)-\eta^3_n(\mathbf{r},t)\right]
\end{aligned} \tag{9}$$

We have chosen to link our phase-field code to the commercial CALPHAD software Pandat (CompuTherm, LLC). The coupling between the phase-field simulation and the commercial thermodynamic database involves the evaluation of the partial derivatives of the local chemical free energy with respect to the eight site fractions ($y^s_n(\mathbf{r},t)$) by Pandat. These partial derivatives are then used to evaluate the partial derivatives of the local chemical free energy with respect to the phase-field parameters, i.e. concentration parameters ($x_n(\mathbf{r},t)$) and the *lro* parameters ($\eta^1_n(\mathbf{r},t), \eta^2_n(\mathbf{r},t), \eta^3_n(\mathbf{r},t)$), through the chain rules:

$$\begin{aligned}
\frac{\partial f}{\partial x_p} &= \sum_{s=1}^{4}\sum_{n=1}^{2}\frac{\partial G}{\partial y^s_n}\frac{\partial y^s_n}{\partial x_p} \ldots p = 1,2,3; \\
\frac{\partial f}{\partial \eta^k_p} &= \sum_{s=1}^{4}\sum_{n=1}^{2}\frac{\partial G}{\partial y^s_n}\frac{\partial y^s_n}{\partial \eta^k_p} \ldots k = 1,2,3.
\end{aligned} \tag{10}$$

The diffusion mobility M_{ij} varies with composition and structure. Due to very limited data on the diffusion mobility of the ordered phase, most simulations to date have used the diffusion mobility of the disordered fcc phase to represent that of the overall behavior of the alloys. In other words, the contribution from the ordered phase is totally ignored although it is well understood that the diffusion behavior and therefore the closely related diffusion mobility in the ordered phase are quite different from that in the disordered fcc phase. Most recently, Campbell has developed a diffusion mobility database that is capable of describing the diffusion mobilities in the γ' phase in the Ni-Al-Cr system [6]. In this work, we adopted this database for the description of the diffusion mobilities in the Ni-Al-Cr system.

The diffusion mobility is expressed as [7]

$$M_{AlAl} = \frac{1}{V_m} x_{Al} \left[x_{Cr} x_{Al} B_{Cr} + (1 - x_{Al})^2 B_{Al} + x_{Al} x_{Ni} B_{Ni} \right]; \tag{11}$$
$$M_{AlCr} = \frac{1}{V_m} x_{Al} x_{Cr} \left[-(1 - x_{Al}) B_{Al} - (1 - x_{Cr}) B_{Cr} + x_{Ni} B_{Ni} \right];$$
$$M_{CrCr} = \frac{1}{V_m} x_{Cr} \left[x_{Al} x_{Cr} B_{Al} + (1 - x_{Cr})^2 B_{Cr} + x_{Ni} x_{Cr} B_{Ni} \right],$$

where B_i is the atomic mobility of species i. The atomic mobility is usually expressed as:

$$B_i = \frac{1}{RT} exp\left(-\Delta Q_i^* / RT\right), \tag{12}$$

where R is the gas constant and Q_i^* is the total activation energy of species i that consists of contributions from the disordered (ΔQ_i^{dis}) and ordered (ΔQ_i^{ord}) states as described below,

$$\Delta Q_i^* = \Delta Q_i^{dis} + \Delta Q_i^{ord}. \tag{13}$$

The contribution from the disordered state, ΔQ_i^{dis}, and its composition dependence can be obtained based on Engstrom and Agren's work [8]. The contribution from the ordered state is described below as in Campbell's work [6],

$$\begin{aligned} \Delta Q_m^{ord} = & \sum_i \sum_{j \neq i} \Delta Q_{i:j}^m [y_i^\alpha y_j^\beta - x_i x_j] + \sum_i \sum_j \sum_k \Delta Q_{ij:k}^m [y_i^\alpha y_j^\alpha y_k^\beta - x_i x_j x_k] \\ & + \sum_i \sum_j \sum_k \Delta Q_{k:ij}^m [y_i^\beta y_j^\beta y_k^\alpha - x_i x_j x_k], \end{aligned} \tag{14}$$

where the index $m, i, j, k = 1, 2, 3$ representing the three components Al, Cr, Ni in the ternay system. y_i^α is the site fraction of component i on the α sublattice that can be readily converted from the current 4-sublattice formulation [9]. $\Delta Q_{i:j}^m, \Delta Q_{ij:k}^m, \Delta Q_{k:ij}^m$ are the contributions to the activation energy for component m as a result of the chemical ordering of the i, j, and k atoms on the two sublattices. These parameters are well documented in Campbell's work [6].

3 Simulation Results and Discussion

As mentioned in the introduciton, the Cr-trapping may be attributed to three factors, i.e. (a) smaller diffusivity of Cr, (b) some kind of favorable initial nucleus structural/compositional profiles, and (c) smaller thermodynamic driving force for Cr diffusion. Simulations are set up to examine how these three factors affect the evolution of Cr concentration in the γ'-precipitates with their growth. Varying diffusivity from benchmark NIST database values is applied for examining factor (a). The results demonstrate that diffusivity alone can not explain the Cr-trapping phenomenon. For factor (b), some representative

structural/compositional profiles need to be chosen to study their effect and some rationale is given below for the choices. The contribution of the thermodynamic driving force is analysed in terms of its gradient and compared with that of the diffusivity for examining factor (c).

For a binary Ni-Al system, homogeneous nucleation is considered the dominant mechanism for γ'-precipitate nucleation. Thermal fluctuation is usually involved in the formation of an enriched Al embryo with L12-type ordered structure, which serves as a potential nucleus. In numerical simulations, such a nucleus is usually represented by an equilibrium γ'-precipitate that is fully ordered and at equilibrium composition. The situation becomes more complex in a multicomponent system. Take the current ternary system Ni-Al-Cr as an example, it is not clear whether it is necessary to have fully ordered Al and Cr simultaneously and at their respective equilibrium compositions in the nucleus for it to survive. Another question is how the structural/compositional environment surrounding a nucleus (in the matrix) such as a partially ordered matrix will affect the survivability of the nucleus and its growth. To answer these questions, it is necessary to study the effect of non-equilibrium structural/compositional profiles in the nucleus and matrix on the growth of precipitates and associated Cr concentration evolution.

In our phase-field representation of the two phase (γ and γ') microstructure, two concentration variables and two sets of ordering parameters (for Al and Cr respectively) are employed. There are many possible combinations as initial profiles for the precipitate (γ') and matrix (γ). For the precipitate, it can be assumed with different degree of ordering of Al and Cr for testing the effect of partial ordering or different degree of ordering in the two species; and various concentrations of Al and Cr to take into account the kinetic effect (e.g. smaller diffusivity of Cr) on the nucleus formation. While the matrix can reasonably be assumed with bulk concentrations, it may still have various degree of ordering especially for Al based on experimental evidence [3], which may affect the growth kinetics of the precipiate and associated Cr concentration evolution with its growth. In this work, the case with fully ordered Al and Cr and equilibrium concentrations in the γ'-precipitate, along with disordered Al and Cr and bulk concentrations in the γ-matrix is chosen as a benchmark case. This case is referred to as case (i) hereafter for convenience of further discussion. Other cases examined in this work include the followings: (ii) fully ordered Al and Cr and measured γ'-nucleus composition by Sudbrack et al. for the precipitate [1], along with disordered Al and Cr and bulk concentrations in the γ-matrix; (iii) partially ordered (50%) Al and Cr and equilibrium concentrations in the γ'-precipitate, along with disordered Al and Cr and bulk concentrations in the γ-matrix; (iv) fully ordered Al and Cr and equilibrium concentrations in the γ'-precipitate, partially ordered Al (50%) and disordered Cr and bulk concentrations in the γ-matrix; (v) homogeneous and disordered Cr in the whole simulation cell, fully ordered Al and equilibrium

concentrations in the γ'-precipitate and disordered and bulk concentration in the γ-matrix. The concentration and the *lro* profiles of these five cases are schematically illustrated in Fig. 1 with a γ'-precipitate located in the center.

The simulations have revealed that the Cr-trapping can only be reproduced with no significant partitioning of Cr at nucleation stage. This is a major factor that contributes to the Cr-trapping. Another factor is related to the composition-dependent diffusivity of Al and Cr. The key difference resides in the much stronger composition dependence of the diffusivity of Al. The diffuvisity of Al is enhanced by approximately an order of magnitude across regions that have significant concentration inhomogeneity such as near or at a γ/γ' interface, a factor that is ignored by mean field approaches. In contrast, the diffusivity of Cr is not at all sensitive to the variation in concentration inhomogeneity. This is another major factor that has caused the Cr-trapping phenomenon.

Fig. 2 shows the growth of a single precipitate (top row) and evolution of Cr concentration with time in the precipitate for five different initial structural/compositional profiles described above. The experimentally measured Cr concentration evolution is also included for comparison. As can be seen, the Cr concentration in the first four cases, i.e. cases (i) through (iv), tends to increase with time with growth of γ'-precipitate, which is the opposite of the experimentally observed trend as shown in Fig. 2(d). A decreasing Cr concentration with time is observed in case (v) where there is no partitioning of Cr in the nucleus. Similar trend is also found with the growth of multiple precipitates (Fig. 3) where cases (i) and (v) are included. For the multiple precipitate case, nuclei are introduced into individual cells randomly, but with the probability related to the corresponding nucleation rate for those cells [10][11][12]. These results suggest that the experimentally observed trend of decreasing Cr in the precipitate with its growth is related to the lack of partitioning of Cr in the nucleation stage.

It was pointed out that a slightly higher diffusivity of Al relative to Cr is not significant enough to be the sole factor to result in the decreasing Cr concentration in the precipitate with its growth. To validate this assessment, some simulations are carried out by varying the chemical mobility of Cr $\left(M^{Ni}_{CrCr}\right)$ (decreasing for the purpose of exaggerating the difference in diffusivity between Al and Cr) that in turn varied (decreased) the diffusivity of Cr since the diffusity is proportional to the mobility, while keeping the original chemical mobilities of Al $\left(M^{Ni}_{AlAl}\right)$ and the cross term $\left(M^{Ni}_{AlCr}\right)$ unaltered. Fig. 4 shows the simulated evolution of Cr with the chemical mobility of Cr set at a half of the literature value [4], which means that the difference of intrinsic diffusivities of Al and Cr are now doubled. This may account for the possible disparity between experimental value and thermodynamically assessed value due to gradient effect. As can be seen, the mobility (diffusivity) change slightly

affected the rate of evolution of Cr for the five cases with different initial nucleus profiles but did not alter the trend even with the current exaggerated difference in mobility (diffusivity). This proves that the diffusivity alone can not explain the Cr-trapping phenomenon.

To gain insight about the respective contribution of chemical mobility and thermodynamic driving force to the Cr-trapping, examination of the two key mobility terms $\left(M^{Ni}_{AlAl}, M^{Ni}_{CrCr}\right)$ and the gradient of the thermodynamic driving force $\left(\nabla \frac{\delta F}{\delta X_j}\right)$ are carried out. Fig. 5 shows the mobility profiles (top row) and the ratio of $M^{Ni}_{CrCr}/M^{Ni}_{AlAl}$ (bottom row) along the middle cross section of the simulation cell. Only cases (i) and (v) (refer to Fig. 1) are included in the chart. The three other cases present almost identical profiles as the case started with equilibrium nucleus, i.e. case (i). The results show a significant increase in Al mobility in the core of the precipitate and interface region. While the value of M^{Ni}_{AlAl} is slightly higher than that of M^{Ni}_{CrCr} in the matrix, the difference is greatly increased in the interface region especially at earlier stages(Fig. 5(a)). In case (i) with equilibrium nucleus, the Al mobility M^{Ni}_{AlAl} in the core of the precipitate is tripled while the Cr mobility is slightly decreased. In case (v) with no partitioning of Cr, although the the Cr mobility is doubled in the core of the precipitate, the Al mobility M^{Ni}_{AlAl} is in contrast increased by roughly an order of magnitude. As a result, the ratio of the two mobilities $(M^{Ni}_{CrCr}/M^{Ni}_{AlAl})$ in both cases is decreased significantly leading to a relatively much higher diffusion rate of Al in the interface region (see Fig. 5(c)). With the growth of the precipitate particle, the compositions at both sides of the interface approach to equilibrium. As a result, the mobility profiles are similar for the two cases at later stages (Fig. 5(b)). However, the enhancement of Al diffusion in the interface region still exists as evidenced by the the ratio of the two mobilities $M^{Ni}_{CrCr}/M^{Ni}_{AlAl}$ in Fig. 5(d).

Fig. 6 shows the gradient of the thermodynamic driving force. It is evident that only the interface region has shown significant gradient of the thermodynamic driving force. The magnitude of the gradient for Al evolution in the interface region is comparable with that for Cr evolution in the whole growth process of the precipitate as represented by the two different stages. As expected, the gradient of the thermodynamic driving force near the interface region is greater for both solutes at earlier stages and it decreases monotonically with the growth of the precipitate and the system is approaching to equilibrium state as shown in Fig. 6(b).

The diffusion rates, i.e. $\partial x_{Al}/\partial t$ and $\partial x_{Cr}/\partial t$), are proportional to a combined term of the chemical mobilities and gradient of thermodynamic driving forces as shown on the right hand side of Eq. 2. The diffusion rates are shown in Fig. 7, which represent effective driving force for diffusions. The effective driving force exists only near the interface region where a mixture of two phases present. It is higher in value in the earlier stage due to higher degree of non-equilibrium

status and it decreases and eventually diminishes at later stages as the system approaches to equilibrium status. This is evidenced by the two snapshots at two representative stages in Fig. 7(a) and (b). Comparing the effective driving force for Al and Cr, it is significantly higher for Al. For example, the effective driving force for Al is approximately one order of magnitude higher than that of Cr for case (v). For case (i), the effective driving force for Cr diffusion is essentially zero while that for Al is moderate. It should be pointed out that the difference in effective driving force for Al and Cr is largely due to the greatly enhanced diffusivity in the interface region for Al. This in turn leads to a much faster diffusion of Al relative to Cr and leaving the Cr behind the interface to 'catch up' later, thus causing the Cr-trapping phenomenon.

Considering that the much enhanced chemical mobility difference in the γ/γ' interface region is the major factor for the Cr-trapping, it is anticipated that this Cr-trapping phenomenon decreases or even disappears if the chemical mobility difference is eliminated. A simulation is run to test this with the chemical mobility of Cr set equal to that of Al, i.e. $M^{Ni}_{CrCr} = M^{Ni}_{AlAl}$, while the cross term M^{Ni}_{AlCr} keeps unchanged. This has in effect increased the chemical mobility (diffusivity) of Cr. The results are shown in Fig. 8, where cases (i) and case (v) are included. For comparison, the two cases shown in Fig. 2(c) are also included as references, where diffusion mobilities from literature databases [6] are used. For case (i) where the nucleus has equilibrium composition and equilibrum *lro* configurations, the evolution of Cr is very similar to that in the reference case. For case (v) where homogeneous Cr is assumed, a rapid decrease of Cr is observed in the first few hours and stays flat from there. In the reference case, however, a steady decrease of Cr concentraion is observed in the whole time window (approximately 300 hours of aging) of the simulations. This result indicates that Cr-trapping may not be 'captured' experimentally due to shortened time window even if no partitioning of Cr occured during nucleation stage, which is not likely to occur considering that the lack of partitioning of Cr is also partially attributed to its lower diffusivity.

Enhanced diffusivity in the γ/γ' interface region is shown to operate to give a substantial increase in the diffusion kinetics of Al over what would be expected from mean field modeling. While the concentration profiles in the interface region are largely controlled by the interplay between interfacial energy and chemical bulk energy, the bulk composition is nevertheless one of the most important factor to determine the actual local compositions in the interface region. Given a different bulk composition as we studied here, the degree of enhancement of Al vs. Cr diffuvisity in the interface region can be decreased or even reversed. An example of such is shown in Fig. 9 for the mobility profiles in a different alloy, i.e. Ni-15Al-5Cr. As can be seen, the diffusivity of Al in the interface region is significantly decreased, which is the opposite of what we observed in the Ni-5.2Al-14.2Cr alloy as shown in Fig. 5. The relative mobility of $M^{Ni}_{CrCr}/M^{Ni}_{AlAl}$ is actually increased slightly in the interface region as shown

in Fig. 9(c),(d). These results indicate that the Cr-trapping phenomenon is strongly tied to the selected compositions of the alloy.

Phase-Field modeling indicates that the Cr-trapping can only be observed for non-equilibrium critical nucleus concentrations. Thermodynamic modeling was employed to show that non-equilibrium critical nucleus concentrations were possible. Following is a discussion of the results that lead us to making this conclusion.

$T_\circ$ is calculated using the built-in thermodynamic database and the result is shown in Fig. 10. In the chart, a shaded zone is plotted that roughly represents possible nucleus concentrations that can survive. The triangle zone is bounded by the $T_\circ$ curve, which determines if the nucleus is energetically favorable, the tie-line and the line with no partitioning of Cr. The tie-line represents an extreme case where the diffusivity of both Al and Cr are so high that it is pure thermodynamic effect in controlling nucleus concentrational profile. On the other hand, the line with no partitioning of Cr represents another extreme case where the diffusivity of Cr is so small that it is totally left out in the formation of the nucleus.

4 Summary

The Cr-trapping phenomenon in Ni-Al-Cr alloys is studied applying a recently developed ternary phase-field model. The effect of the compositional/ordering profiles of the nucleus and the diffusivity on the evolution of Cr concentration in the γ' precipitate is simulated. The simulation work reveals that the Cr-trapping phenomenon can only be reproduced with no significant partitioning of Cr at the nucleation stage. This is belived to be a major factor that causes the Cr-trapping observed by experiments. Another factor is related to the much stronger composition-dependent diffusivity of Al as compared to Cr for the alloy composition under investigation. The diffuvisity of Al is enhanced by approximately an order of magnitude across regions that have significant concentration inhomogeneity at a γ/γ' interface. In contrast, the diffusivity of Cr is not much affected in the interface region. This is another major factor that has caused the Cr-trapping phenomenon.

Acknowledgements

We appreciate the helpful discussions with Dennis Dimmiduk at AFRL. Computations were performed at the ASC high performance computing center.

YHW acknowledges support from the Air Force Research Laboratory (AFRL) through contract #F33615-01-C-5214 with UES Inc.

References

[1] C.K. Sudbrack, R.D. Noebe, and D.N. Seidman. *Acta mater.*, 54:3199, 2006.

[2] Y.H. Wen, J. Lill, S.L. Chen, and J.P. Simmons. *Acta mater. submitted*, 2008.

[3] C.K. Sudbrack, R.D. Noebe, and D.N. Seidman. *Phys Rev B*, 73:212101, 2006.

[4] N. Saunders. *in Superalloys*, page 101. TMS, 1996.

[5] J. W. Cahn and J. E. Hilliard. *J. Chem. Phys.*, 28:258, 1958.

[6] C.E. Campbell. *Acta mater.*, doi:10.1016/j.actamat.2008.04.061, 2008.

[7] JO Andersson and J. Agren. *J. appl. phys.*, 72:1350, 1992.

[8] A. Engstrom and J. Agren. *Z. Metallkd*, 87:92, 1996.

[9] I. Ansara, N. Dupin, H.L. Lukas, and B. Sundman. *J. alloy compd.*, 247:20, 1997.

[10] J.P. Simmons, C. Shen, and Y. Wang. *Scripta mater.*, 43:935, 2000.

[11] Y.H. Wen, J.P. Simmons, C. Shen, C. Woodward, and Y. Wang. *Acta metall.*, 51:1123, 2003.

[12] Y.H. Wen, B. Wang, J.P. Simmons, and Y. Wang. *Acta metall.*, 54:2087, 2006.

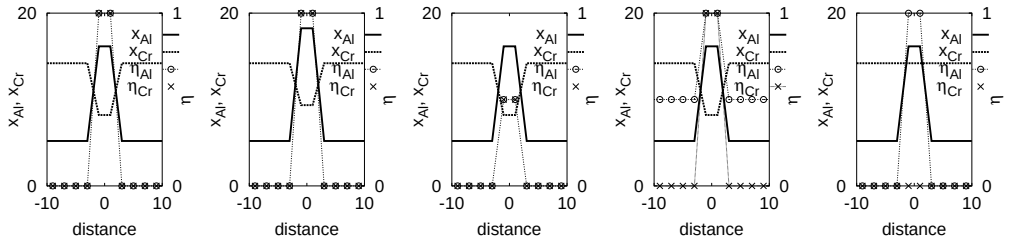

Fig. 1. Illustration of the five initial structural/compositional profiles tested in this work.

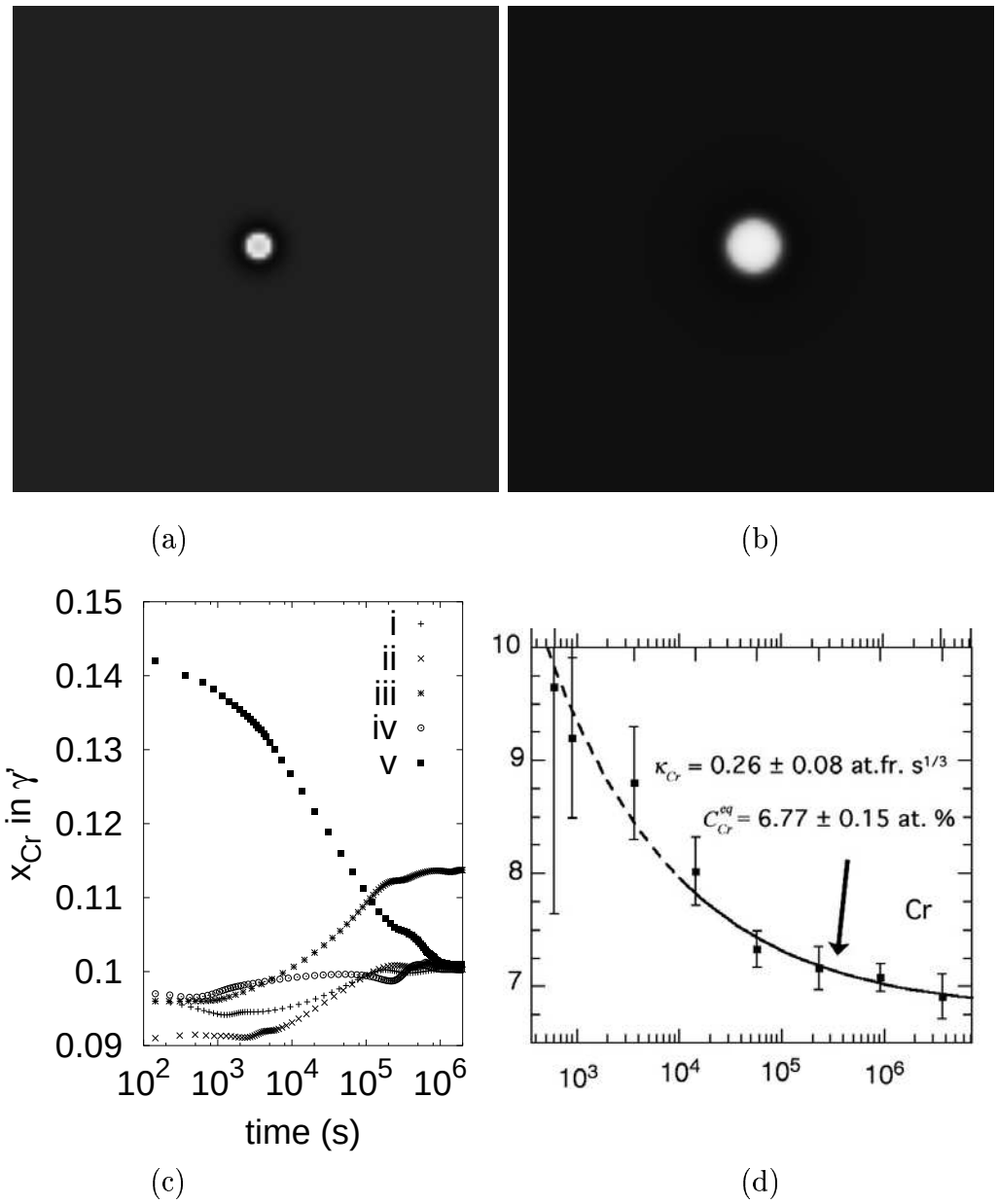

Fig. 2. Effect of initial nucleus structural/compositional profiles on Cr concentration evolution in a single precipitate: A snapshot of the precipitate at the earlier (a) and later stage of the simulation (b), simulated evolution of Cr concentration with time (c) and expermentally observed Cr concentration evolution (d).

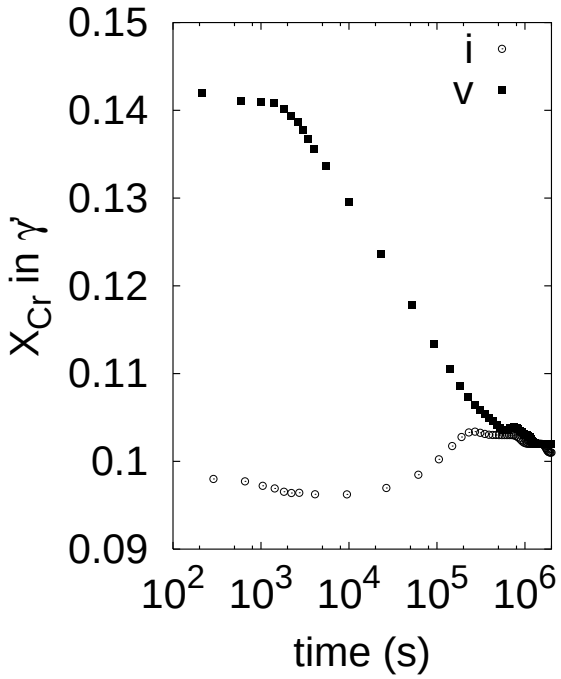

Fig. 3. Effect of initial nucleus structural/compositional profiles on Cr concentration evolution in multiple precipitates.

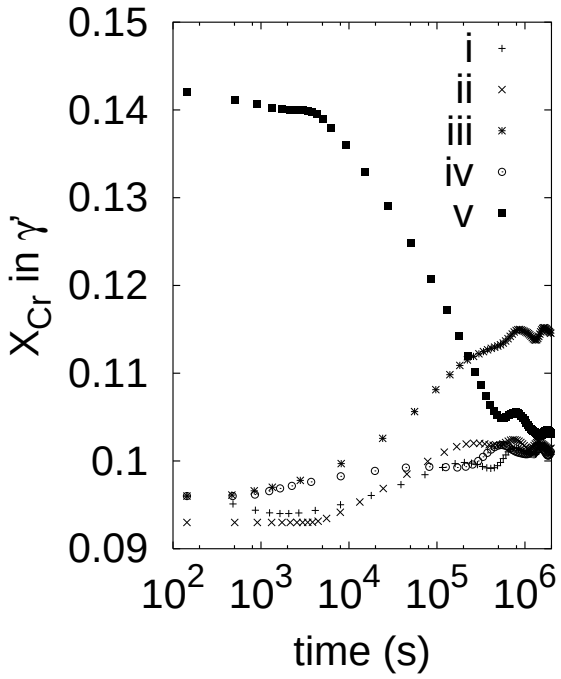

Fig. 4. Mobility effect on Cr concentration evolution in a single precipitate.

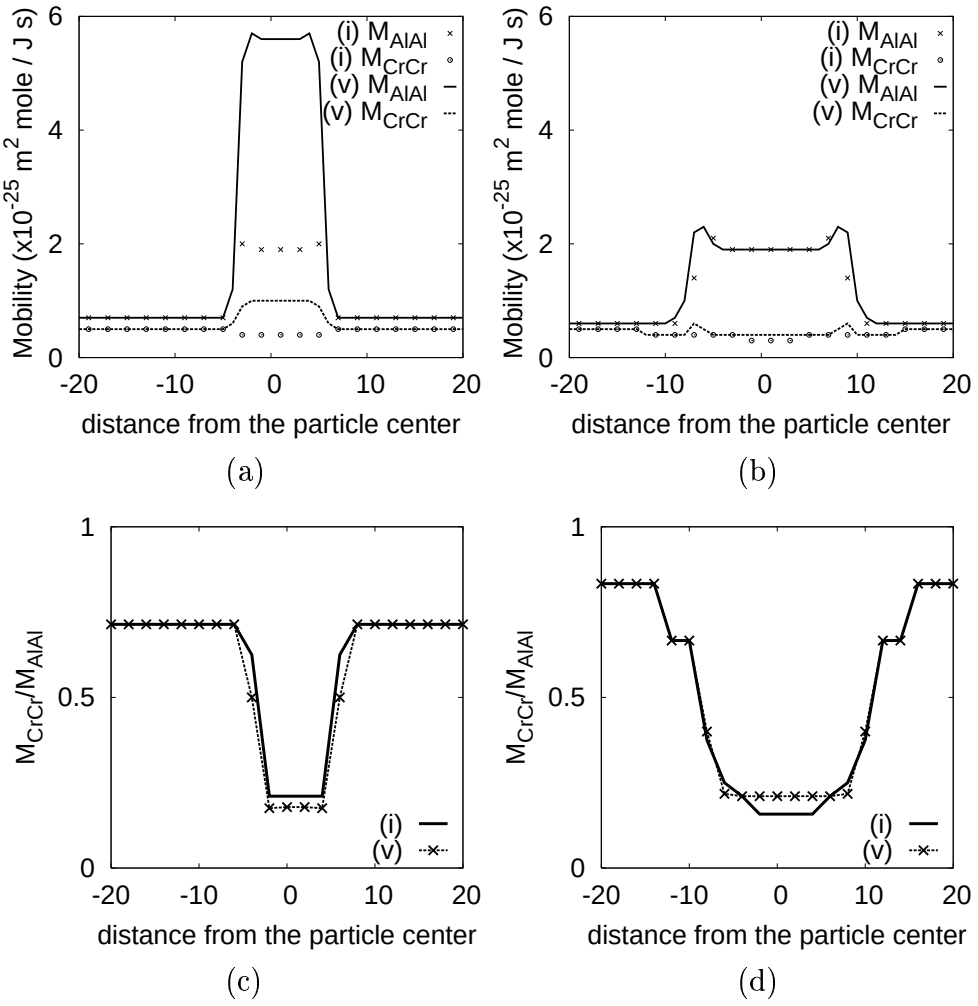

Fig. 5. Profiles of the mobility (top row) and the ratio of $M^{Ni}_{CrCr}/M^{Ni}_{AlAl}$ (bottom row) for cases (i) and (v) along the middle horizontal cross-section: (a) and (c) earlier stage at t=0.2 (h); (b) and (d) later stage at t=70 (h).

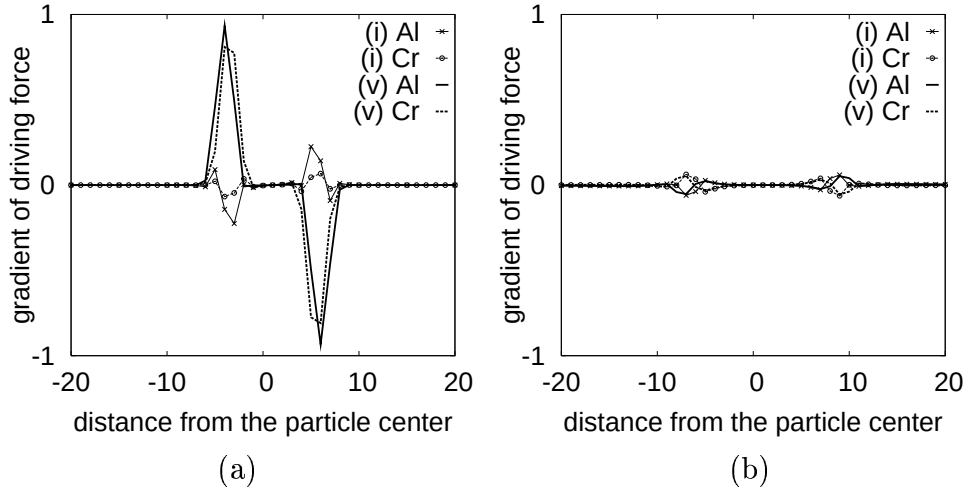

Fig. 6. Profiles of the gradient of the thermodynamic driving force for cases (i) and (v) shown in Fig. 2(b) along the central portion of the middle horizontal cross-section: (a) earlier stage at t=0.2 (h), (b) later stage at t=70 (h).

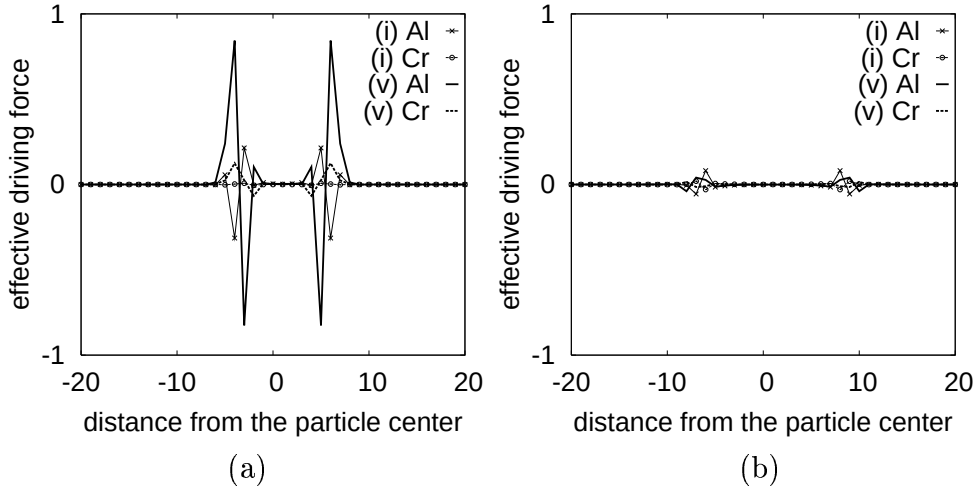

Fig. 7. The concentration evolution rate profile for Al and Cr for cases (i) and (v) shown in Fig. 2(b) along the middle horizontal cross-section: (a) earlier stage at t=0.2 (h), (b) later stage at t=70 (h).

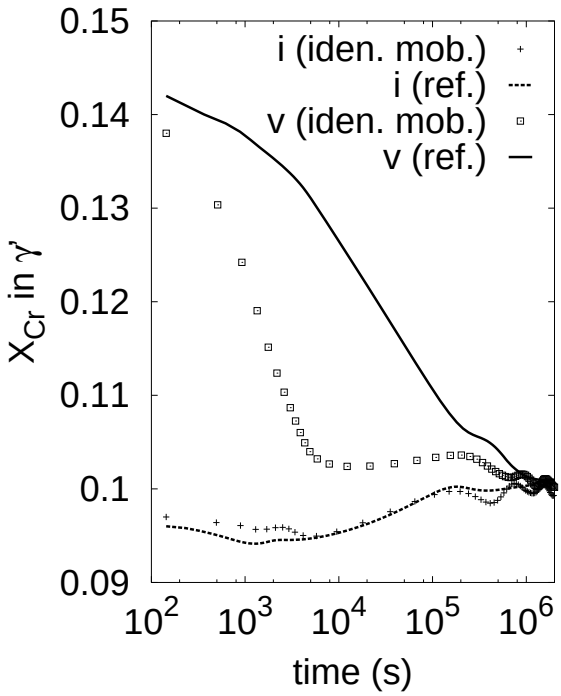

Fig. 8. *Cr* concentration evolution in a single precipitate with the mobility of *Cr* set to equal to that of *Al*. Reference cases are included for comparison where the diffusion mobilities from literature database are used.

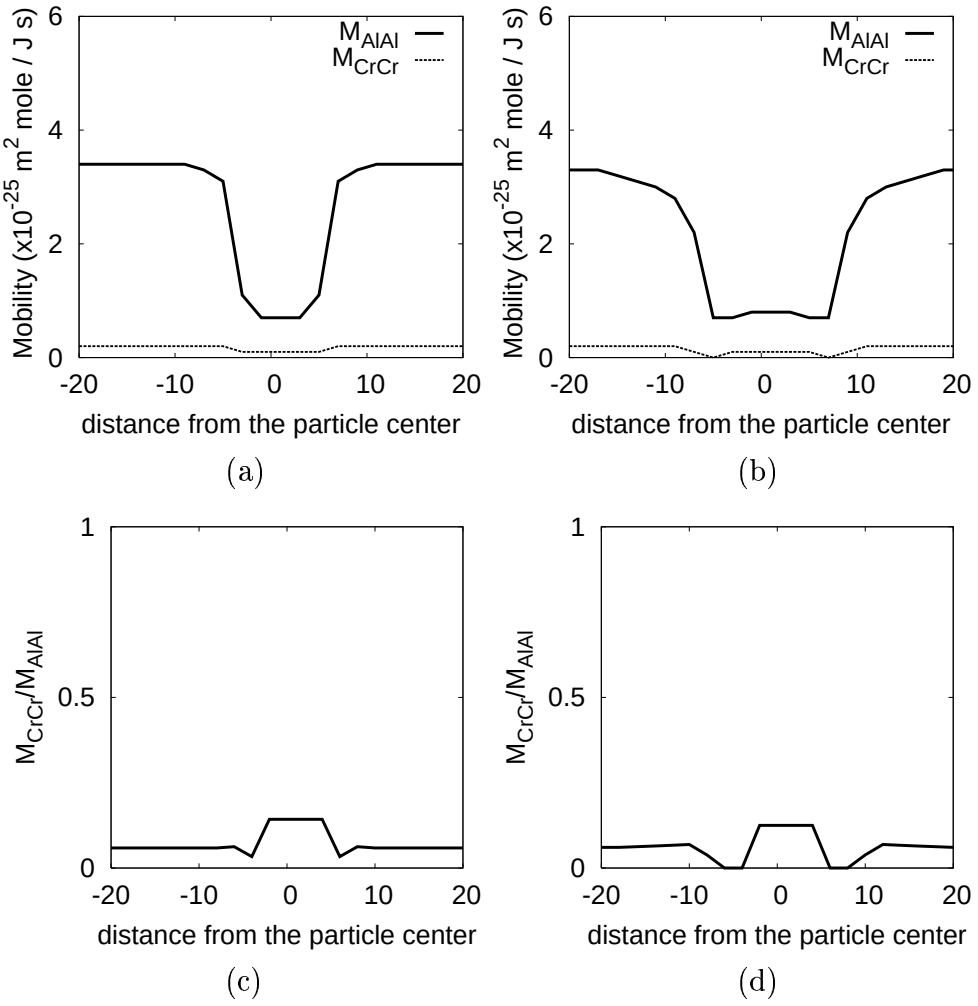

Fig. 9. Profiles of the mobility (top row) and the ratio of $M^{Ni}_{CrCr}/M^{Ni}_{AlAl}$ (bottom row) in Ni-15Al-5Cr alloys along the middle horizontal cross-section: (a) and (c) earlier stage at t=0.2 (h); (b) and (d) later stage at t=10 (h).

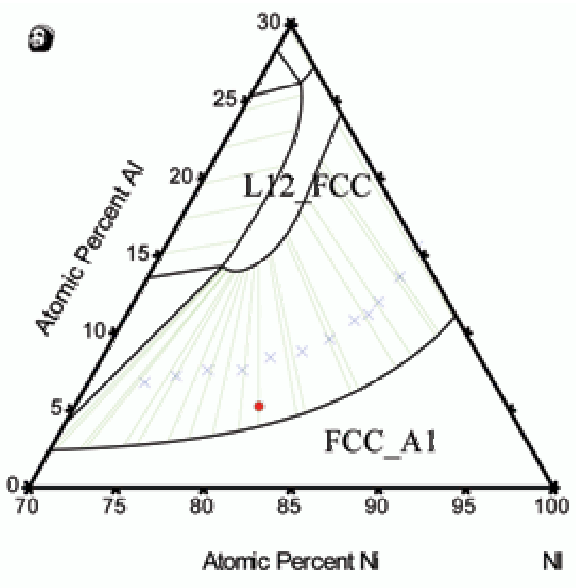

Fig. 10. Calcualted $T_\circ$ curve and projected survivable nucleus concentration region.